Jurnal Tribologi 29 (2021) 41-56

MYTRIBOS Malaysian Tribology Society

Jurnal Tribologi

Website : jurnaltribologi.mytribos.org e-issn: 2289-7232

# Microstructures generated by nickel aluminium bronze alloy L-PBFed and their effect on tribological and mechanical properties

Fathia Alkelae *, Shinya Sasaki

Sasaki Laboratory, Department of Mechanical engineering, Tokyo University of Science, 6-Chome-3 Niijuku, Katsushika, Tokyo 125-8585, JAPAN.
*Corresponding author: alkelae.fathia@gmail.com

KEYWORDS

Additive manufacturing
L-PBF
Friction
Nickel aluminum bronze
Wear
Phase nucleation
Heat treatment

ABSTRACT

High density nickel-aluminium bronze alloy (Cu9Al4Fe3Ni) was manufactured using Laser powder-bed fusion technique (L-PBF), it was investigated regarding the effect of different heat treatment conditions on its mechanical, microstructural and tribological behaviour. Correlations between the microstructures generated ($\kappa$ phases) and the behaviour observed were established. Regardless the heat treatment applied (annealing, tempering, quenching & tempering), friction coefficient, wear loss and hardness have been shown to decrease with increasing heat treatment temperature, while tensile strength and the elongation improved compared to the as-built sample. On the other hand, correlations using increased precipitates content resulting from different heat treatments confirmed the improvement of the material's mechanical properties at the expense of the tribological ones. A possible interpretation of this results maybe the role of precipitates in impeding dislocations motion leading to increased shear forces, thus deteriorating the embeddability of the soft $\alpha$ phase along with detachment of the hard $\kappa$ phases allowing a three-body abrasive wear to occur. However, in a process similar to strain hardening, hardness and tensile strength are shown to improve with increased precipitation.

Received 30 December 2020; received in revised form 24 February 2021; accepted 13 April 2021.
To cite this article: Alkelae and Sasaki (2021). Microstructures generated by nickel aluminium bronze alloy L-PBFed and their effect on tribological and mechanical properties. Jurnal Tribologi 29, pp.41-56.

## 1.0 INTRODUCTION

Nickel aluminium bronze is a category of aluminium bronze alloys consisting of aluminium as the important alloying element ranging from 8 to 12%, iron and nickel with percentages from 3 to 6% each, manganese is added with small amount to improve castability. Despite their percentages difference, this category of alloys shows similar properties. Many industries such as marine applications, electrical contacts, landing gears and bearings make use of this alloy owing to its high corrosion and wear resistance, high mechanical properties and lightweight feature compared to other alloys.

In our previous study (Alkelae et al., 2020), successful manufacturing of the alloy whose chemical composition is shown in Table 1 was achieved using L-PBF technique, results revealed higher mechanical and tribological properties compared to other manufacturing techniques in the as-built condition.

The microstructure of nickel aluminium bronze (NAB) may show various phases depending on the manufacturing technique and the cooling rates applied. In addition to the martensitic $\beta'$ phase, the high temperature $\beta$ phase and the lamellar $\alpha$ phase, $\kappa$-phases also may be generated as highlighted by the alloy phase diagram shown in Figure 1, the green area demarcates the domain of this category (NAB) of aluminium bronze family. These phases are different in shape, chemical composition and properties (Scudino et al., 2015; Culpan et al., 1978).

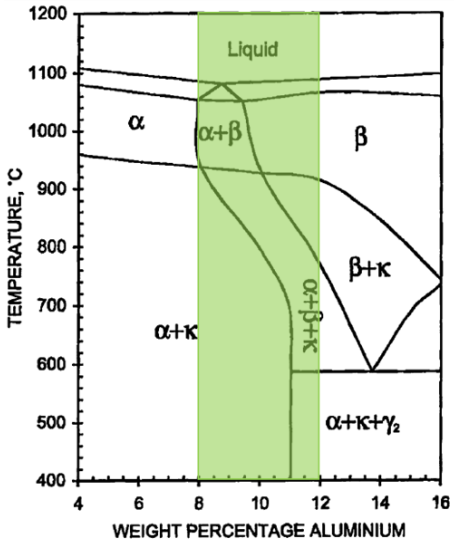


Figure 1: Phase diagram of nickel-aluminum bronze alloy (Culpan et al., 1978).

Generally, there is 4 kinds of $\kappa$-phases as shown in Figure 2 along with their formation temperatures. $\kappa_I$-phase forms when iron content is higher than 5 wt.% [Hasan et al., 2018, Anantapong et al., 2014], coarse and globular in shape (Figure 2), they precipitate at higher temperature before precipitation of $\alpha$ phase, when they form, they give rise to $\alpha$ phase upon cooling. Having ordered bcc structure, they can precipitate as $Fe_3Al$ or FeAl. At 900°C precipitation of $\kappa_{II}$-phase ($Fe_3Al$) begins initially in the $\beta$ phase and develops in $\alpha$ phase, it is found at the boundary of $\beta/\alpha$ phases along with $\kappa_{III}$-phase which starts precipitating between 840°C and

600°C. $\kappa_{III}$ are a nickel-rich particles (NiAl), lamellar or globular in shape depending on solidification conditions, increasing nickel and aluminium content or decreasing iron content favour their formation. They are reputed for improving the proof strength of the alloy. $\kappa_{IV}$-phase is a finely divided iron-rich particles in the $\alpha$ phase ($Fe_3Al$ with bcc structure), they can appear if the cooling rate is sufficiently slow (Meigh., 2008), the strength and hardness of the alloy get improved by their precipitation (Kamran et al., 2018).

Microstructural analysis showed that upon rapid cooling during L-PBF process, freezing of the microstructure occurs yielding mainly $\beta'$ phase and some lamellar $\alpha$ phase. Knowing that nickel aluminium bronze can generate various phases during solidification capable of further improving the properties of the alloy, specific heat treatments were applied in order to enhance the alloy's performance.

In the following, some specific heat treatments will be applied aiming to yield $\kappa$-phases. A full investigation will be conducted regarding the effect of every phase on the mechanical and tribological properties of the alloy. Kamran et al. (Kamran et al., 2018) showed that phases do not have the same improvement behaviour on the alloy properties. Mechanical properties may be enhanced at the expense of tribological ones and vice versa. Furthermore, some phases have higher improvement effect than others as highlighted in Nascimento et al. investigation (Nascimento et al., 2019). The objective of this paper is to obtain the best combination of phases allowing improvement of both mechanical and tribological properties, taking as a reference, the combination of properties obtained in the as built condition.

Table 1: Chemical composition of Ni-Al-Bronze alloy used in this study (Alkelae et al., 2020).

| **Al-Bronze** | Al | Fe | Ni | Zn | P | Pb | Sn | O | Mn | Cu |
|---|---|---|---|---|---|---|---|---|---|---|
| **Mass %** | 9.56 | 4.2 | 3.39 | 0.28 | 0.02 | 0.012 | 0.082 | 0.09 | 0.843 | balance |

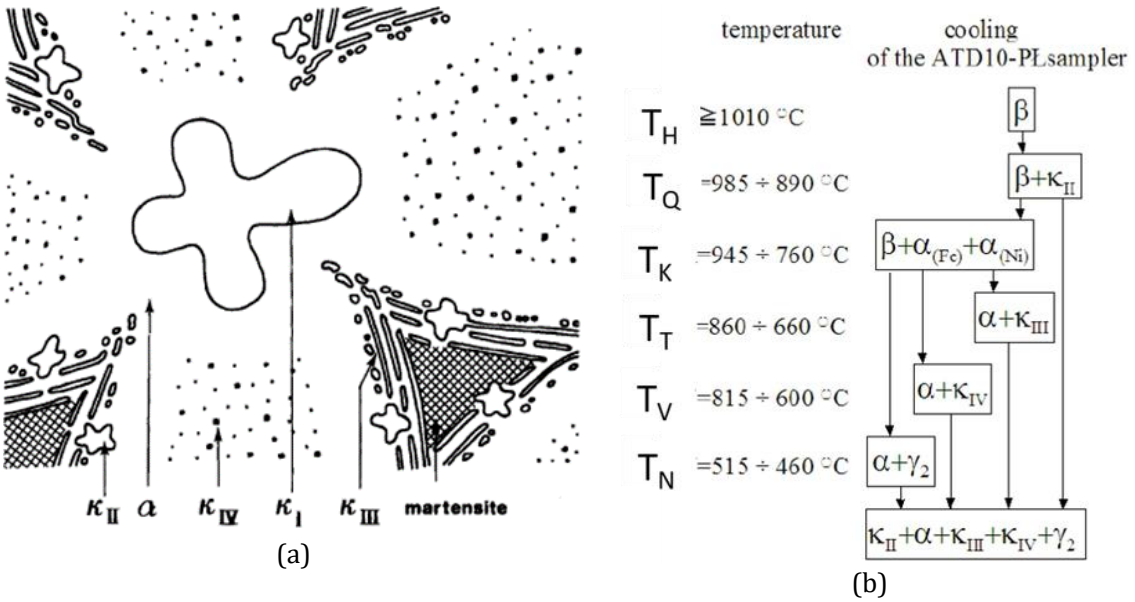


(a) (b)

Figure 2: (a) Schematization of different NAB phases (Hasan et al. 1982) and (b) temperature formation and precipitation of NAB phases during cooling (Pisarek, 2013).

## 2.0 EXPERIMENTAL PROCEDURE

L-PBF manufacturing was successfully conducted using a laser power of P = 260 W, a scanning velocity v = 600 mm/s, a hatch space h= 120 µm and a layer thickness of t = 30 µm (E =120.37 J/mm$^3$) is the best combination allowing obtention of higher densities for this alloy ( $\rho \geq 94$ %).

This study aims to disclose the effect of various microstructures on the overall behaviour of nickel aluminium bronze alloy. To achieve our objective which is defining the best heat treatment regarding mechanical and tribological properties, appropriate heat treatments were performed for specific microstructures generation as shown below:

H.T.:1 Heating at 600°C for 1 hour followed by air cooling (tempering)
H.T.:2 Heating at 700°C for 2 hours followed by air cooling (tempering)
H.T.:3 Heating at 850°C for 1hour, quenched in water, heating at 720°C for 5hours followed by air cooling (Quenching + tempering)
H.T.:4 Heating at 930°C for 30min followed by furnace cooling (annealing)
H.T.:5 Heating at 980°C for 2hours followed by furnace cooling (annealing)
H.T.:6 Heating at 980°C for 2hours, followed by furnace cooling till 600°C, followed by air cooling (annealing)

After each heat treatment, microstructural analyses were performed using FE-SEM (FE-SEM Supra40, Carl Zeiss, Germany) equipped with energy dispersive X-ray spectroscopy (EDS-Quantax Esprit 1.9, Bruker, Germany). Etching with a solution composed of 5g of $Fe_3Cl$, 10 ml of HCl and 100 ml of distilled water was conducted with a reaction time of 20 seconds. The same characterization strategy is adopted here as for our previous investigation (Alkelae and Sasaki 2020).

Tensile samples (Figure 3a) were manufactured with respect to ISO standard for strength measurements, with a width of 3.5 mm, a thickness of 3.5 mm, a round section of 20 mm radius and a grid section length of 12 mm. Tests were performed at a speed of 1 mm/s (AG-10 kNX plus, Shimadzu, Japan). Vickers hardness was measured with micro–Vickers Hardness Tester (HMV-G-FA-D, Shimadzu, Japan) in order to evaluate the bulk material's hardness. For friction tests (SRV4, Optimol instruments, Germany), discs were manufactured according to their maximum density (95%) as shown in Figure 3b.

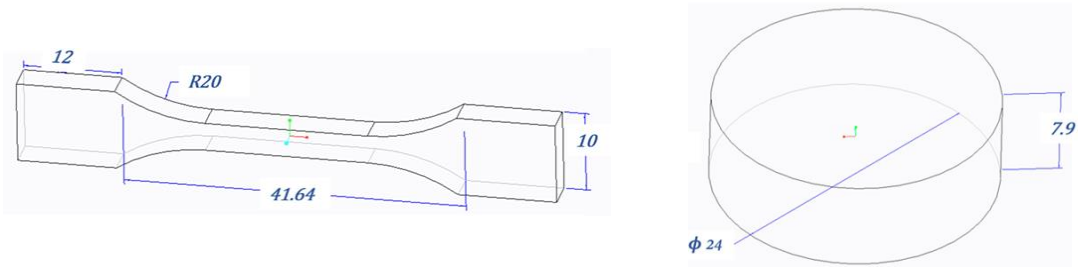


(a) (b)

Figure 3: Samples used for the investigation: (a) for tensile testing and (b) for friction tests (cylinder on disc configuration) (Alkelae and Sasaki 2020).

The manufactured discs were heat treated and polished prior to friction tests. Other samples were prepared for etching in order to reveal the generated microstructure for each heat treatment condition. Wear volume was measured by a Laser microscope (VK-X150, Keyence, Japan). X-Ray diffraction analyses were conducted in order to reveal the formed phases (SmartLab 9Kw, Rigaku, Japan). Comparison between the as-built sample (Alkelae and Sasaki 2020) and the heat-treated specimens is considered to evaluate the effect of heat treatment on the alloy's behaviour.

## 3.0 RESULTS AND DISCUSSION

### 3.1 FE-SEM Analysis

Heat treatments are applied to nickel aluminium bronze alloys aiming to eliminate the corrosion prone eutectoid phase $\boldsymbol{\alpha + \gamma_2}$ leading to degradation of mechanical properties (Culpan et al., 1978), in addition to precipitation of the hard $\boldsymbol{\kappa}$-phases. In a study conducted by Pisarek (Pisarek, 2013) for a cast Ni-Al bronze (Cu-11Al-6Ni-5Fe), a very interesting model was established, where the author unraveled the crystallization and phase transformation temperatures of different microconstituents (based on thermal and derivative analysis, TDA). In this study, some heat treatments are proposed to nucleate different $\boldsymbol{\kappa}$-phases in order to evaluate their effect on mechanical and tribological properties of our additively manufactured alloy. According to the model, precipitation of phases is ranged as follows:

$\boldsymbol{\kappa_{III}}$: from 660°C to 860°C
$\boldsymbol{\kappa_{IV}}$: from 600°C to 815°C
$\boldsymbol{\kappa_{II}}$: from 890°C to 985°C

Tempering at 600°C yields a rich microstructure of needle-like $\boldsymbol{\alpha + \kappa_{III}}$ as shown in Figure 4a, increasing the temperature from 600°C to 700°C along with time at temperature (from 1 hour to 2 hours) has a coarsening effect on the $\boldsymbol{\kappa_{III}}$ phase. This explains the drop in tensile strength and hardness as well as the friction coefficient (please refer to Table 3). Fast cooling (air cooling) promotes $\boldsymbol{\kappa_{III}}$ particles formation. Depending on temperature and time at temperature, these particles may be coarse or fine. Finer particles improve mechanical properties at the expense of tribological ones. Quenching and fast cooling (Figure 4c) yields $\boldsymbol{\kappa_{IV}}$ and $\boldsymbol{\kappa_{II}}$ particles, lower friction coefficient and wear loss are observed compared to previous heat treatments. Upon slow cooling (Furnace cooling), $\boldsymbol{\kappa_{II}}$ particles form leading to further improvement of tribological properties. Globular $\boldsymbol{\kappa_{III}}$ are also observed owing to the slow cooling rates as confirmed by Lin (Lin et al., 2016).

The solubility of iron in $\boldsymbol{\alpha}$ phase is exceeded at 850°C (Jahanafrooz et al., 1983) (860°C for Anantapong. (2014)). In the case of slow cooling, formation of $\boldsymbol{\kappa_{II}}$ and $\boldsymbol{\kappa_{IV}}$ takes place at high temperatures while upon rapid cooling $\boldsymbol{\kappa_{III}}$ forms, however, quenching at 850°C followed by tempering at 720°C does not generate $\boldsymbol{\kappa_{III}}$ precipitates. We can deduce that at high temperatures and slow cooling rates, the spherical precipitates form while formation of the lamellar precipitates form upon rapid cooling from lower temperatures (600°C and 700°C). Through his investigation, Jahanafrooz et al. (1983) has concluded that the higher the temperature at which the $\boldsymbol{\alpha}$ phase forms, the higher its iron content. This elucidates the absence of $\boldsymbol{\kappa_{IV}}$ upon tempering at 600°C and 700°C. Increasing the heat treatment temperature to 850°C and 930°C increases the solubility of iron in $\boldsymbol{\alpha}$ leading to precipitation of $\boldsymbol{\kappa_{IV}}$ and $\boldsymbol{\kappa_{II}}$.

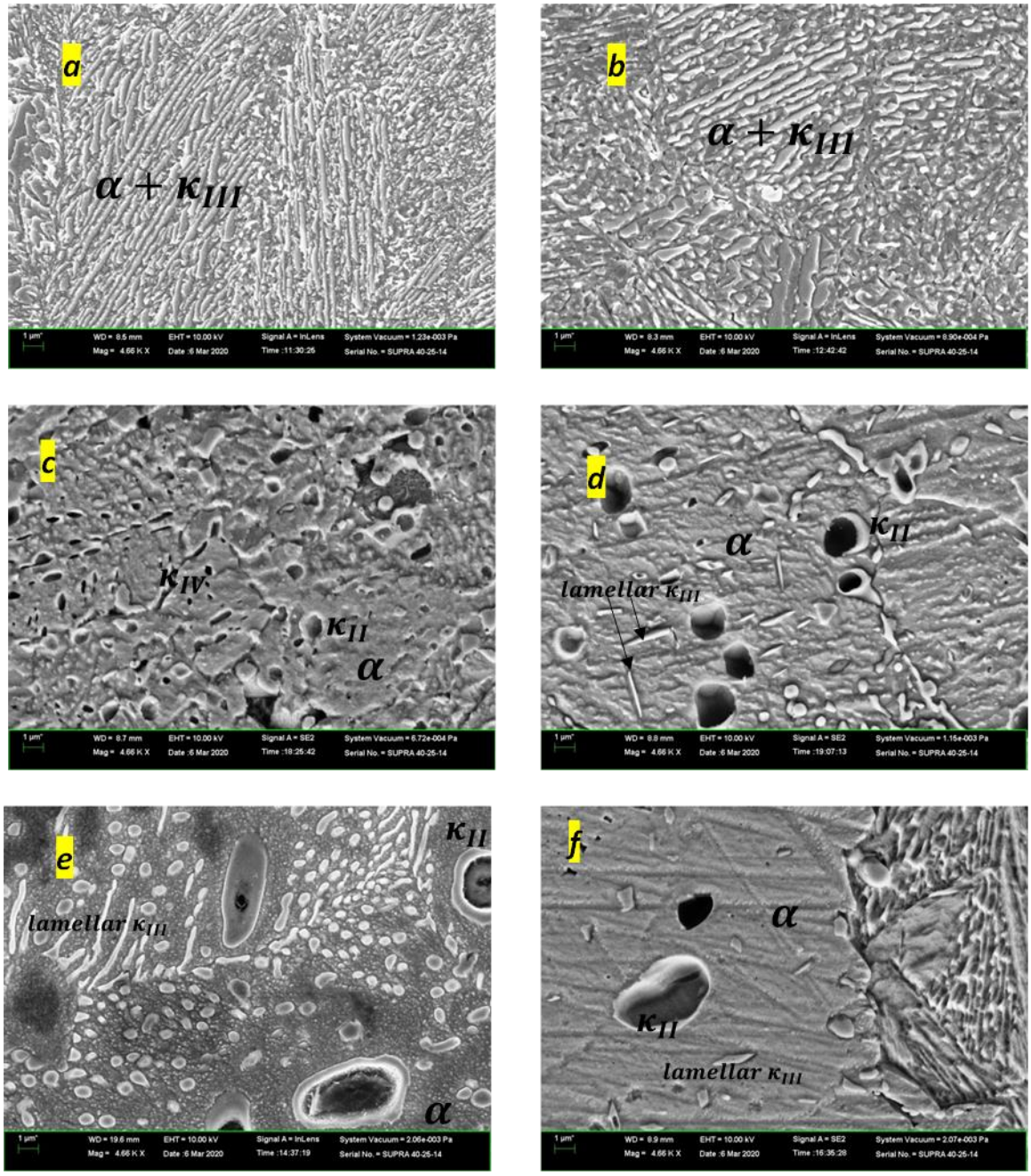


Figure 4: FE-SEM micrographs of etched samples upon various heat treatments, (a) tempered at 600°C for 1 hour, (b) tempered at 700°C for 2 hour, (c) quenched from 850°C (after holding time of 1 hour) and tempered at 720°C for 5 hours, (d) furnace cooled from 930°C with 30min holding

time, (e) furnace cooled from 980°C after 2 hours holding time and (f) furnace cooled from 980°C (after holding time of 2 hours) to 600°C and then air cooled.

According to Pisarek, (2013), upon cooling the solubility of Al in $\boldsymbol{\beta}$ phase increases leading to diffusion of Al in the $\boldsymbol{\beta}$ grains and dealuminizing the boundary, thus transforming it into $\boldsymbol{\alpha}$ ($\boldsymbol{\beta} == > \boldsymbol{\beta} + \boldsymbol{\alpha}$), the high excess of Al in $\boldsymbol{\alpha}$ phase is resent to $\boldsymbol{\beta}$ phase by diffusion and locates in the front of its crystallized grains, upon cooling the $\boldsymbol{\alpha}$ phase (Ni-rich $\boldsymbol{\alpha}$) nucleates and grows as $\boldsymbol{\kappa_{III}}$ (NiAl). This transformation is situated between 660°C and 860°C, while for Anantapong it is observed at 800°C (Anantapong et al., 2014).

Several EDS analyses were performed for each heat treatment on the precipitated phases aiming to reveal their chemical composition. Table 2 summarizes the averaged results for each phase (considering all heat treatments applied). Culpan, (1978) showed through analyzing intensively $\boldsymbol{\kappa}$ phases (20 to 30 times) that chemical composition of a phase may change from sample to another and even within the same sample, thus, elucidating the fact that these phases can exist within a large range of chemical composition even if they have precipitated at the same temperature from the matrix.

Table 2: Chemical composition of different phases encountered with the applied heat treatments.

| Phase | Chemical composition (wt%) | | | | |
|---|---|---|---|---|---|
| | **Cu** | **Al** | **Fe** | **Ni** | **Mn** |
| α | 89.32904 | 6.364469 | 1.035875 | 2.563847 | 0.706772 |
| Retained β | 84.27795 | 7.323211 | 3.514275 | 4.154185 | 0.730382 |
| $\kappa_{II}$ | 21.62±7.69 | 18.98±2.13 | 35.75±6.03 | 21.53±3.68 | 2.09±0.46 |
| $\kappa_{III}$ | 37.80±11.33 | 19.49±6.94 | 19.83±5.28 | 20.92±4.22 | 1.94±0.49 |
| $\kappa_{IV}$ | 27.62±3.91 | 19.63±4.01 | 30.13±4.45 | 20.75±3.64 | 1.85±0.24 |

### 3.2 Tribological Characterization

To elucidate the effect of heat treatments applied and the resulting microstructures on tribological properties of Ni-Al bronze, lubricated friction tests were conducted under the same conditions used for the as-built sample (50 N, 50 Hz, 1000 $\mu m$ sliding distance, 80°C and 1hour test duration). Further details may be found in (Alkelae et al., 2020), using cylinder on disc configuration. The friction coefficient evolutions are depicted in Figure 5, the mean friction coefficient values are listed in Table 3. For the first three heat treatments (tempering and quenching-tempering), fluctuant evolutions and high friction coefficients are observed. This may be due to the presence of hard particles at the interface. On the other hand, relatively low and smooth evolutions are observed while annealing from high temperatures with the last three heat treatments. Wear scars were also analyzed using FE-SEM, showing some interesting results in good agreement with the frictional behavior. For the first three heat treatments (Figure 6: a, b and c), the unstable evolution of the friction coefficient is due to the presence of a rough area containing protrusions generated from the severe abrasive and adhesive wear mechanism. The stable evolution of friction coefficient of the last three heat treatments (Figure 6: d, e and f) is obviously due to the smooth wear scars, confirming the dominant adhesive wear mechanism. Generally, wear loss decreases with high temperatures (Table 3) generating low precipitates content as highlighted in Table 4. Tao (Tao et al., 2018) also confirmed that the increase in $\kappa$ phases increases the wear rate of specimens.

EDS analysis were performed considering the typical surfaces (rough and smooth). The results are depicted in Figure 7. At higher applied temperatures (heat treatments: 4, 5 and 6), the alumina formed before testing is very adherent to the substrate making the evolution of friction coefficient very stable as seen in Figure 5: d, e and f, in that case (smooth surfaces case), an increase of both iron and oxygen concentrations is observed suggesting formation of a transfer film from the counterbody. On the other hand, with lower heat treatments temperatures, alumina film breaks up easily as we can see from EDS mapping (Figure 7), owing to its hardness, three body abrasive wear mechanism takes place leading to fluctuant friction evolution (Figure 5-a, b and c).

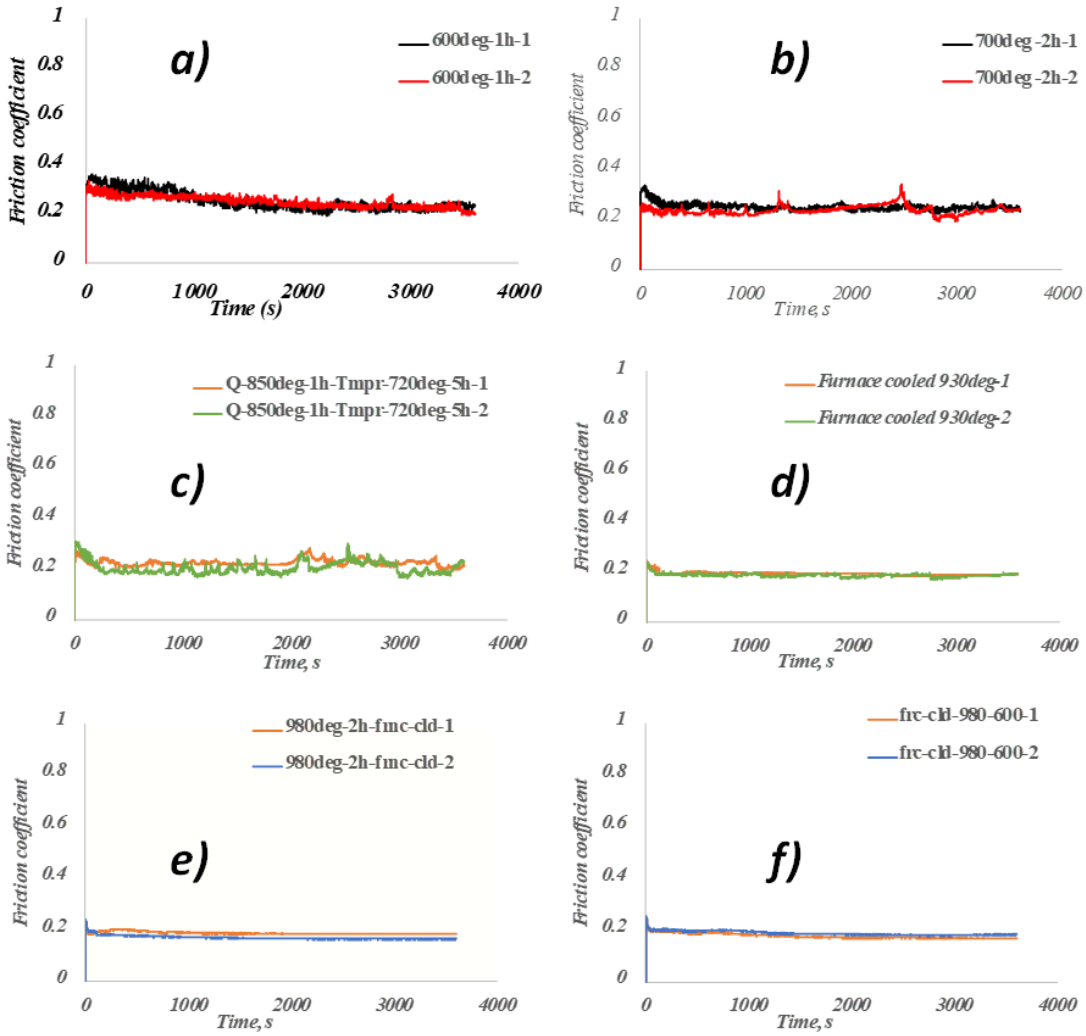


Figure 5: Friction coefficient evolutions under the heat treatments considered in this study, (a) tempered at 600°C for 1 hour, (b) tempered at 700°C for 2 hour, (c) quenched from 850°C (after holding time of 1 hour) and tempered at 720°C for 5 hours, (d) furnace cooled from 930°C with 30min holding time, (e) furnace cooled from 980°C after 2 hours holding time and (f) furnace cooled from 980°C (after holding time of 2 hours) to 600°C and then air cooled.

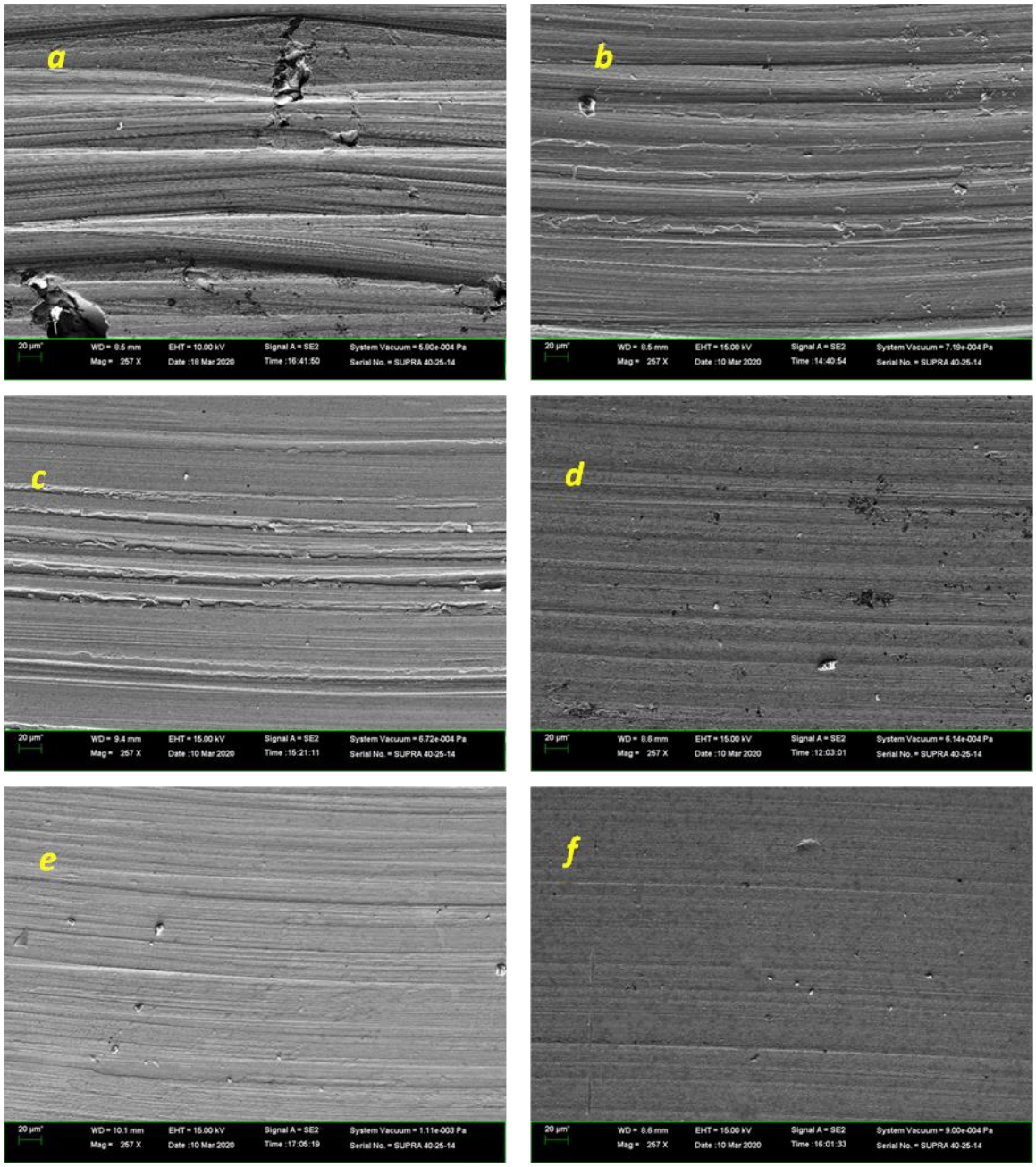


Figure 6: Wear scars observation under the heat treatments considered in this study, (a) tempered at 600°C for 1 hour, (b) tempered at 700°C for 2 hour, (c) quenched from 850°C (after holding time of 1 hour) and tempered at 720°C for 5 hours, (d) furnace cooled from 930°C with 30min holding time, (e) furnace cooled from 980°C after 2 hours holding time and (f) furnace cooled from 980°C (after holding time of 2 hours) to 600°C and then air cooled.

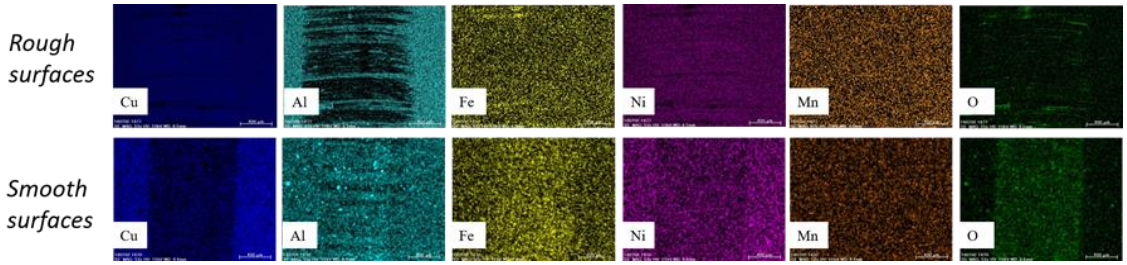


Figure 7: EDS mapping of typical wear scars: rough surfaces and smooth surfaces.

### 3.3 Mechanical Characterization

The results of tensile tests and hardness measurements after each heat treatment are shown in Table 3, a maximum of strength is obtained by tempering at 600°C for 1hour. According to XRD and phase quantification results (Table 4), this heat treatment generates more precipitates than others, progressive decrease in strength is observed with decreasing the total precipitates content regardless their nature. This may be interpreted by the decreased effect of strengthening due to decreased content of precipitates. Furthermore, if we refer to Figure 4, we can see clearly that with globular precipitates ( $\kappa_{II}$ ), the microstructure is characterized by voids suggesting detachment of precipitates, however, with lamellar precipitates ($\kappa_{III}$), no voids are found, this observation may lead to think that the lamellar precipitates cannot be detached assuming their high resistance to deformation, thus imparting the material a high strength.

Similarly, the hardness is shown to decrease with increasing heat treatments temperature, according to Table 4, the decrease of hardness is accompanied by decreased precipitated particles, which confirms that the particles nature is unlikely to play a role, since both lamellar and spherical particles if precipitated by the same amount, same hardness value is obtained, viz: HV = 205 (H.T.:2 yields 16% of lamellar precipitates Vs H.T.:3 yielding also 16% of precipitates globular in nature). However, the maximum hardness is obtained with the as-built sample, this means that the $\beta'$ microstructure generated upon the very fast cooling rate is harder than a microstructure of $\alpha$ combined with the precipitated $\kappa$ phases. With heat treating, transformation of $\beta$ into $\alpha$ and $\kappa$ phases is induced, thus reducing the amount of retained $\beta$ or martensitic $\beta'$ phase, as a result, lower hardness is obtained. The elongation, on the other hand, is influenced by the nature of precipitates as we can see with both heat treatments H.T.:2 and H.T.:3 with same amounts of precipitates. The globular precipitates impart higher elongation to the material compared to the lamellar ones. The maximum elongation is obtained with the highest amount of $\alpha$-phase (23%).

Comparing the heat treatment at 930°C for 30 min followed by furnace cooling to the study of Kamran et al. (Kamran et al., 2018) who applied the same heat treatment, L-PBF provides higher hardness with a microstructure containing $\kappa_{II}$ and $\kappa_{IV}$ phases against only $\kappa_{II}$ obtained with the hot forged sample.

Table 3: Results of mechanical and tribological properties with the applied heat treatments.

| | **Friction coefficient μ** | **Wear Volume (mm³)** | **Tensile strength (MPa)** | **Hardness $V_H$** | **Elongation %** |
|---|---|---|---|---|---|
| AS-BUILT SAMPLE | 0.2±0.003 | 0.191±0.006 | 479±13.39 | 393±28.86 | 1.49±0.07 |
| H.T.: 1 | 0.252±0.002 | 0.100±0.005 | 794±4.43 | 267±29.85 | 3.38±0.001 |
| H.T.: 2 | 0.244±0.007 | 0.106±0.034 | 654±0.66 | 205±28.74 | 14.81±0.18 |
| H.T.: 3 | 0.216±0.009 | 0.097±0.002 | 571±3.27 | 205±2.42 | 18.21±0.32 |
| H.T.: 4 | 0.191±0.003 | 0.108±0.041 | 524±5.1 | 193±4.2 | 17.91±0.3 |
| H.T.: 5 | 0.179±0.008 | 0.03±0.0015 | 531±8.4 | 162±16.17 | 18±0.03 |
| H.T.: 6 | 0.184±0.005 | 0.016±0.004 | 525±1.5 | 167±16.76 | 23±3.06 |

### 3.4 XRD Analysis

After each heat treatment, X-ray diffraction (SmartLab, Rigaku, Japan) tests were conducted without any pre-processing to avoid altering the microstructure orientations and stress state, the scans were performed in the $2\theta$ range from 5° to 120°, using Cu $K_\alpha$ radiation ($\lambda = 1.54\ A^{\circ}$). PDXL software was used to identify (based on fitting the peaks with that of ICCD, PDF-2 release 2014 RDB) and quantify the precipitated phases (based on Reference Intensity Ratio method), the results are shown in Figure 8 and Table 4.

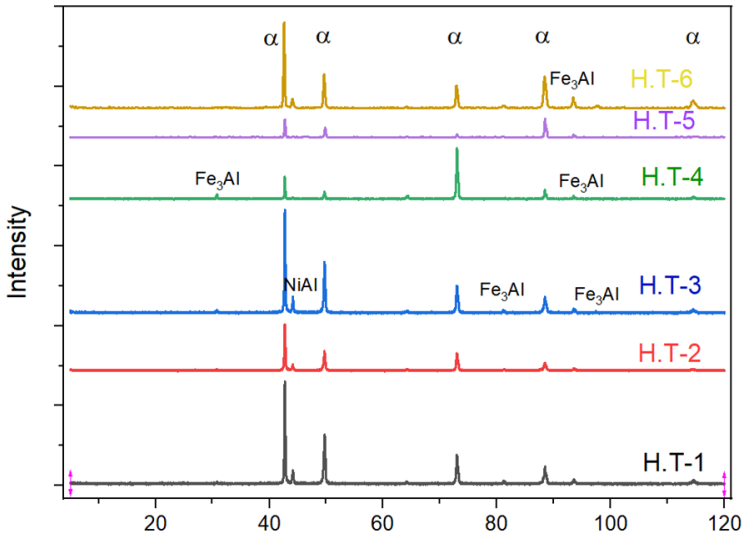


Figure 8: XRD patterns of heat-treated samples.

The main peak of all samples is that of copper $\alpha$-rich phase with various magnitudes depending on heat treatment applied, $\kappa$ phases are represented by $Fe_3Al$ for $\kappa_{II}$ and $\kappa_{IV}$ (distinguished by their shape and size based on microstructural observations, and temperature range formation based on Pisarek model as described above) and NiAl for $\kappa_{III}$. The quantification in Table 4 supports X-ray diffraction analysis, only the Cu-rich $\alpha$ phase, $Fe_3Al$ and NiAl peaks are present and detected. The increase of heat treatment temperatures shifts the $Fe_3Al$ peak to higher

angles, from 30° with annealing from 930°C to 95° and 100° with annealing from 980°C. The pattern of the annealed sample from 980°C till 600°C followed by air cooling (980°C-2h- Frn-cld to 600°C -air-cld) reflects the peaks of the Cu-rich $\alpha$ phase, according to the quantification results, this alloy contains 96% of $\alpha$ phase.

Table 4: Phases quantification for each applied heat treatment.

| Phase | Heat treatment | | | | | |
|---|---|---|---|---|---|---|
| | **H.T.:1** | **H.T.:2** | **H.T.:3** | **H.T.:4** | **H.T.:5** | **H.T.:6** |
| α | 75.14 % | 88.1 % | 83.5 % | 89 % | 89 % | 96.04 % |
| $\kappa_{II}$ | | | 9.63 % | 11 % | 10 % | 2.97 % |
| $\kappa_{III}$ | 23.12 % | 16.4 % | | | 1 % | 0.99 % |
| $\kappa_{IV}$ | 1.73 % | | 7.02 % | | | |

## 4.0 DISCUSSION

In his review, Brezina (Brezina., 2013) confirmed that quenching followed by tempering of nickel aluminium bronze produces the highest mechanical properties. He also stated that redistribution of stacking faults along with annealing of dislocations occur at first stages of tempering allowing obtention of maximum strength values, slightly above this critical time the strength decreases accompanied with important improvement in ductility. In the present study the maximum tensile strength and hardness are obtained with tempering heat treating for 1 hour at 600°C, upon which a very fine microstructure of $\alpha + \kappa_{III}$ is generated. On the other hand, an $\alpha$-rich microstructure with $\kappa_{II}$ and $\kappa_{IV}$ was obtained with quenching and tempering imparting lower mechanical properties to the material. These results show that L-PBF followed by heat treatments yields different microstructures than expected when processing with conventional manufacturing techniques. This discord may only originate from the use of L-PBF that guarantees formation of a martensitic microstructure with the highest amount of dislocations compared to other manufacturing techniques, thus serving as nucleation sites of fine precipitates upon heat treatments.

Regardless the heat treatment applied (tempering, quenching and tempering, annealing), as much as the temperature increases, the friction coefficient decreases along with the wear loss and the hardness, whereas the strength goes to its maximum with H.T.: 1 (up to ≈ 800 MPa) before following the same trend as other properties with increased heat treatment temperature. On the other hand, the elongation keeps improving with increasing the temperature with a maximum of 23 % with H.T.: 6, this improvement is proportional to the increased amount of $\alpha$ phase.

As we investigated our alloy upon the applied heat treatments, we first of all elucidated the precipitation hardening effect of different phases compared to the as-built sample as follows:

An improvement of tensile strength by 165% is observed with fine $\alpha + \kappa_{III}$ $(lamellar)$, by 136 % with coarse $\alpha + \kappa_{III}$ $(lamellar)$, by 119 % with $\alpha + \kappa_{II} + \kappa_{IV}$, by 109 % with $\alpha + \kappa_{II}$ and by 110 % with $\alpha + \kappa_{III}$ $(globular) + \kappa_{II}$.

Strengthening is related to the amount and size of precipitates ($\kappa$-phases). The hardness is shown to decrease with increased heat treatment temperature, this is due to recrystallization and coarsening of grains with the applied heat treatments and stresses relaxation compared to the as-built sample. Yuting (Lv et al., 2015) investigated the difference in microhardness of friction stir processed NAB (Cu9.5Al4.2Ni4Fe1.2Mn) using transmission electron microscopy (TEM), the

results showed that the obtained microstructure consisted of high quantity of dislocations and high amount of $\beta'$ phase. Moreover, annealing leads to discontinuous static recrystallization and coarsening, decreased amount of $\beta'$ phase and decreased dislocations quantity thus decreasing the work-hardening effect, which explains the decrease in the microhardness of the stirred zone. Shen et al.,(2018) showed that heat treatments leading to significant density of $\kappa$ phases in NAB fabricated by wire arc additive manufacturing (WAAM) yield samples with higher hardness compared to the as-fabricated one, on the other hand, if the density of $\kappa$ phases is low, lower hardness is to be expected. The reverse is observed in this study, the as-built samples not containing any $\kappa$ phases showed the highest hardness. Upon heat treatments, different types of $\kappa$ phases nucleate resulting in lower hardness. In our case $\beta'$ phase transforms completely to $\alpha + \kappa$. $\beta'$ does not seem to contribute to the hardness improvement.

## 5.0 RELATIONSHIP BETWEEN PRECIPITATES AND MATERIAL'S PROPERTIES

Many studies tackled the subject of stacking fault energy (SFE) in copper alloys and its sensitivity to alloying (Gallagher et al.,1970), solute concentration (Buckley., 1967) and temperature (Pineau and Remy., 1978), as well as its effect on friction ( Buckley., 1967), wear and hardness (Wert et al., 1983). In general, alloying with a higher valence solute along with the increase in solute concentration ( Gallagher et al.,1970) decreases the SFE. Remy et al. ((Pineau and Remy., 1978) explained the decrease in SFE with increasing the temperature by the thermal activation of dislocations motion, he also stated that in case the increase of temperature leads to segregation of a solute, this will impede the dislocations motion, leading to local increase of shear forces, thus increasing the friction coefficient. Buckley (Buckley., 1967) studied the effect of increasing the solute concentration at room temperature in order to induce segregation, a decrease in SFE simultaneously with increase in shear forces and friction coefficient were observed. Wert et al (Wert et al., 1983) similarly to Buckley, studied the combined effect of increasing solute concentration and the resulting decrease in SFE, he found that wear rate and bulk hardness along with the hardness in the wear scars increase accordingly.

Knowing that the precipitates play similar role on dislocations motion as solutes and with analogy to previous results, an attempt is made to establish a correlation between the precipitate concentration and nickel aluminium bronze properties such as tensile strength, friction, wear and Hardness.

The material properties were plotted as a function of precipitates content (the sum of all precipitates for each heat treatment calculated in Table 4). Similar trends are obtained as for the correlation with solute concentration, the mechanical properties are shown to improve at the expense of the tribological ones. For the friction coefficient, it is shown that increasing precipitates content increases the friction coefficient, while it decreases with more $\alpha$ phase in the microstructure. In the case of two different heat treatments (tempering at 700°C for 2 hours and quenching tempering) with the same precipitates content, similar friction coefficient is obtained. The hard $\kappa$ phases alter the embeddability of the soft $\alpha$ phase generating an abrasive wear process along with high friction coefficients. On the other hand, enhancement of tensile strength and hardness is granted by the precipitation strengthening effect.

This can be a deciding tool on whether the targeted properties are the mechanical or tribological ones. Keeping more $\alpha$ guaranties higher tribological properties while increasing $\kappa$-phases content improves mechanical properties. Li (Li et al,. 1996) found that the optimum volume ratio of the soft to hard phases is 67:33 besides an $\alpha$ grain size between 33-46 $\mu$m,

adhesive wear is found with higher ratio while abrasive wear dominates with lower ratio. In the same way, Li (Li et al,. 1996) correlated the tribological behaviour and mechanical properties to the content of $\alpha$ phase and the corresponding grain size, he found that the optimal combination of properties is obtained when the volume percent of $\alpha$ phase is 67 % and its grain size is about 35 µm. They referred the sharp increase in wear rate and friction coefficient with a volume percent of $\alpha$ phase from 70 % to 76 % compared to the case with less than 63 % to the sudden decrease in the yield strength of the alloy at these ranges. He also stated that, if the adhesive wear is dominant, increasing the hardness and lowering the plasticity will have an advantageous effect on friction coefficient and wear rate, on the other hand, if the abrasive wear is dominant, increasing the hardness and lowering the plasticity will have a negative effect on tribological properties.

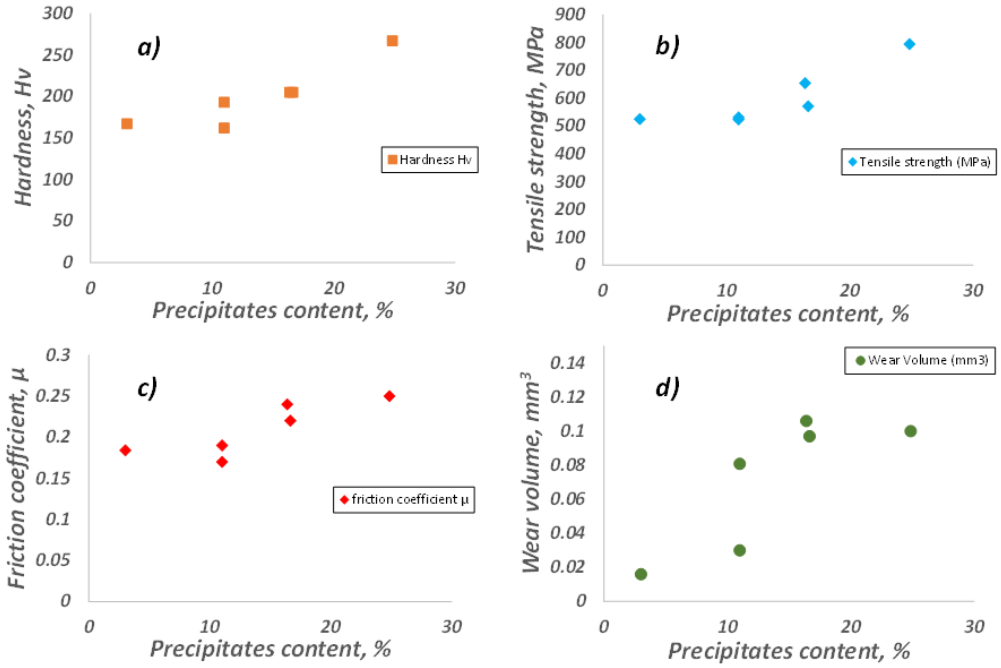


Figure 9: Influence of precipitates content on material properties: (a) on hardness, (b) on tensile strength and (c) on friction coefficient and d) on wear volume.

## 6.0 CONCLUSIONS

By reference to the microstructures obtained with different heat treatments, it is obvious that the single phase offers the best tribological properties at the expense of the mechanical ones, $\alpha$ associated with $\kappa_{II}$ (930°C for 30min furnace cooled) improves moderately the hardness and strength while the friction coefficient and wear loss increase. With the addition of $\kappa_{IV}$ phase (Quenched-tempered HT), further improvement of mechanical properties at the expense of tribological ones is observed. A microstructure consisting of $\alpha + \kappa_{III}$ (tempered at 700°C for 2 hours) caused raising of friction coefficient along with the hardness and yield strength, while the

worst tribological properties and the highest strength are obtained with the finest $\alpha + \kappa_{III} + \kappa_{IV}$ microstructure (tempered at 600°C for 1 hours).

Ranking of friction coefficient regarding the applied heat treatments: $\alpha < \alpha + \kappa_{II} < \alpha + \kappa_{II} + \kappa_{IV} < \alpha + \kappa_{III} < \alpha + \kappa_{III} + \kappa_{IV}$, with the lower value attributed to the microstructure with $\alpha$ phase.

**REFERENCES**

Alkelae, F., & Sasaki, S. (2020). Tribological and Mechanical Characterization of Nickel Aluminium Bronze (NAB) Manufactured by Laser Powder-Bed Fusion (L-PBF). Tribology Online, 15(3), 126-135.

Anantapong, J., Uthaisangsuk, V., Suranuntchai, S., & Manonukul, A. (2014). Effect of hot working on microstructure evolution of as-cast Nickel Aluminum Bronze alloy. Materials & Design, 60, 233-243.

Brezina, P. (1982). Heat treatment of complex aluminium bronzes. International Metals Reviews, 27(1), 77-120.

Buckley, D. H. (1967). Possible relation of friction of copper-aluminum alloys with decreasing stacking-fault energy. National Aeronautics and Space Administration.

Culpan, E. A., & Rose, G. (1978). Microstructural characterization of cast nickel aluminium bronze. Journal of Materials Science, 13(8), 1647-1657.

Gallagher, P. C. J. (1970). The influence of alloying, temperature, and related effects on the stacking fault energy. Metallurgical Transactions, 1(9), 2429-2461.

Hasan, F., Jahanafrooz, A., Lorimer, G. W., & Ridley, N. (1982). The morphology, crystallography, and chemistry of phases in as-cast nickel-aluminum bronze. Metallurgical Transactions A, 13(8), 1337-1345.

Jahanafrooz, A., Hasan, F., Lorimer, G. W., & Ridley, N. (1983). Microstructural development in complex nickel-aluminum bronzes. Metallurgical Transactions A, 14(10), 1951-1956.

Li, Y., & Ngai, T. L. (1996). Grain refinement and microstructural effects on mechanical and tribological behaviours of Ti and B modified aluminium bronze. Journal of materials science, 31(20), 5333-5338.

Li, Y., Ngai, T. L., & Xia, W. (1996). Mechanical, friction and wear behaviors of a novel high-strength wear-resisting aluminum bronze. Wear, 197(1-2), 130-136.

Lin, G., Wang, H., Wei, Y., Zhang, Z., & Zhou, K. (2016). Effects of heat treatments on microstructure and properties of nickel-aluminum bronze fabricated by centrifugal casting. Journal of Materials Research, 31(24), 3832.

Lloyd, D. M., Lorimer, G. W., & Ridley, N. (1980). Characterization of phases in a nickel-aluminium bronze. Metals Technology, 7(1), 114-119.

Lv, Y., Wang, L., Xu, X., & Lu, W. (2015). Effect of post heat treatment on the microstructure and microhardness of friction stir processed NiAl bronze (NAB) alloy. Metals, 5(3), 1695-1703.

Meigh, H. (2018). Cast and wrought aluminium bronzes: properties, processes and structure. CRC Press.

Nascimento, M. S., Santos, G. A. D., Teram, R., Santos, V. T. D., Silva, M. R. D., & Couto, A. A. (2019). Effects of thermal variables of solidification on the microstructure, hardness, and microhardness of Cu-Al-Ni-Fe alloys. Materials, 12(8), 1267.

Pisarek, B. P. (2013). Model of Cu-Al-Fe-Ni Bronze Crystallization. Archives of Foundry Engineering, 13.

Rémy, L., Pineau, A., & Thomas, B. (1978). Temperature dependence of stacking fault energy in close-packed metals and alloys. Materials Science and Engineering, 36(1), 47-63.

Shen, C., Pan, Z., Ding, D., Yuan, L., Nie, N., Wang, Y., ... & Li, H. (2018). The influence of post-production heat treatment on the multi-directional properties of nickel-aluminum bronze alloy fabricated using wire-arc additive manufacturing process. Additive Manufacturing, 23, 411-421.

Tao, X. P., Zhang, S., Zhang, C. H., Wu, C. L., Chen, J., & Abdullah, A. O. (2018). Effect of Fe and Ni contents on microstructure and wear resistance of aluminum bronze coatings on 316 stainless steel by laser cladding. Surface and Coatings Technology, 342, 76-84.

Wert, J. J., Singerman, S. A., Caldwell, S. G., & Quarles, R. A. (1983). The role of stacking fault energy and induced residual stresses on the sliding wear of aluminum bronze. Wear, 91(3), 253-267.

Yaseen, M. K., Mansoor, M., Ansari, H. A., Hussain, S., & Khan, S. (2018). Effect of heat treatment on tribological characteristics of CuAl10Ni5Fe4 nickel aluminum bronze. In Key Engineering Materials (Vol. 778, pp. 61-67). Trans Tech Publications Ltd.